



SU² REAL GAS MODELS' PERFORMANCE PREDICTIONS ON A COLD GAS THRUSTER

Aysu ÖZDEN*, Özgür Uğraş BARAN**, Mehmet Halûk AKSEL*** ve Mehmet Ali AK****

*.***.***Orta Doğu Teknik Üniversitesi Makina Mühendisliği Bölümü, 06800, Ankara

*aysu.ozden@metu.edu.tr, ORCID: 0000-0001-9257-1377

**ubaran@metu.edu.tr, ORCID: 0000-0002-8437-7862

***aksel@metu.edu.tr, ORCID: 0000-0003-0563-4216

**** ROKETSAN A.Ş. Elmadağ, 06780, Ankara

mehmetali.ak@roketan.com.tr ORCID: 0000-0001-8204-8961

(Geliş Tarihi: 22.07.2020, Kabul Tarihi: 25.01.2021)

Abstract: Cold gas propulsion systems are preferred, especially for the altitude and trajectory control for satellites, since the 1960s. Both depressurizing the propellant in the propellant tank throughout the mission and the expansion occurring in the divergent part of the thruster nozzle are the reasons for observing very low temperatures and pressure at the outlet section. We have decided to use an open-source compressible CFD tool, SU², in order to predict the performance of the propulsion system in the early design phase. The scope of this study is the comparison of the results of the vacuum chamber performance tests and the outcomes of unsteady simulations with SU² using different gas models, including ideal gas, van-der Waals, and Peng-Robinson models. Then, the accuracy and performance of these models are evaluated for the extremely low temperature and pressure conditions. Thruster performance tests have been conducted in the thermal vacuum chamber test campaign at the specially built testing facilities. In order to simulate nominal and low-temperature operation conditions, a propellant tank is thermally conditioned to the predetermined values, and performance test parameters are used as the input for the CFD simulations. The obtained results showed that the van der Waals gas model is the most appropriate gas model for both cases and provides the most realistic results in terms of performance parameters.

Keywords: Cold gas thruster, Real gas models, Vacuum chamber test, SU².

SU² GERÇEK GAZ MODELLERİNİN SOĞUK GAZ İTİCİSİ PERFORMANS TAHMİNLERİ

Özet: Soğuk gaz itki sistemleri 1960'lı yıllardan bu yana özellikle uyduların yörünge kontrolünde tercih edilen sistemler olmuşlardır. Yakıt tankındaki yüksek basıncın görev süresince azalması nedeniyle, tank içindeki yakıtta oldukça düşük sıcaklıklar gözlenmektedir. Ayrıca itici lülesinin çıkışında da, vakuma yakın basınçlara genleşen yakıtın sıcaklığı oldukça düşmektedir. Bu koşullar altında, itki sisteminin performansının tasarım sürecinde gerçekçi olarak tahmin edilebilmesi için, açık kaynaklı, sıkıştırılabilir akışkanlar için uygun bir hesaplamalı akışkanlar dinamiği aracı olan SU²'nin kullanılması kararlaştırılmıştır. Bu çalışmada, itki sisteminin doğası gereği karşılaşılan düşük sıcaklık ve basınç etkilerinin doğru modellenebilmesi adına, SU²'nin ideal gaz, van-der Waals ve Peng-Robinson gaz modelleri kullanarak elde edilen performans tahminleri ile itici vakum odası performans test sonuçları karşılaştırılmıştır. İtici performans testleri için bu amaçla kurulan termal vakum odası test alt yapısı kullanılmıştır. İtici simülasyonları ve performans testleri, yakıt tankının nominal ve düşük sıcaklıkta koşulladığı durumlar için yürütülmüştür. Elde edilen veriler, SU² van der Waals gaz modelinin, her iki sıcaklık koşulunda da vakum odası performans testlerine en yakın sonuçları verdiğini göstermektedir.

Anahtar Kelimeler: Soğuk gaz iticisi, Gerçek gaz modelleri, Vakum odası testi, SU².

NOMENCLATURE

CFL Courant-Friedrichs-Lewy number

MFP mean free path

A area [m²]

a measure of intensity of the molecular attraction force

b co-volume

c speed of sound[m/s]

c_p heat capacity at constant pressure [J/molK]

c_v heat capacity at constant volume [J/K]

d_m molecular diameter [Å]

e total energy per unit mass [J/kg]

F thrust [N]

k_b Boltzmann constant [J/K]

Kn Knudsen number

M Mach number

\dot{m} mass flow rate [g/s]

p	pressure [Pa,bar]
R	gas constant [J/kgK]
s	total entropy per unit mass [J/kgK]
T	temperature [K]
V	velocity [m/s]
α	measure of intermolecular attraction force
ρ	density [kg/m ³]
λ	distance traveled by a molecule between two consecutive collisions
λ_n	nozzle efficiency
γ	ratio of specific heats
ν	specific volume [m ³ /kg]
ω	acentric factor
subscripts	
a	ambient
c	chamber
cr	critical value
e	exit
ref	reference value
t	throat

INTRODUCTION

Space exploration has always been at the center of human attention, and one of the most studied space objects has been the satellites since the 1960s. Aim to control satellite maneuverability and trajectory has emerged the need to have a compact and efficient propulsion system. From the beginning, the cold gas propulsion systems have been preferred considering their design simplicity, lower mass, cost-effectiveness and compatibility. Providing low thrust and specific impulse compared to chemical propulsion systems are the primary disadvantages of such systems. However, they are considered broadly in satellite propulsion since their simple construction provides reliability and robustness.

A simple sketch of a cold gas propulsion system is given in Fig. 1. As can be seen from the figure, usually, there is one propellant tank, a pipeline to deliver the propellant to the rest of the system, valves to control the propellant motion and thrusters. Thrusters are the combination of the nozzle and the thruster valve, which allow the propellant to the nozzle. The propellant tank usually contains a high-pressure gaseous propellant, yet the operational pressure level is considerably lower. A pressure regulator is located downstream of the propellant tank to decrease the high pressure in the tank to operational levels. Thrust is obtained by discharging the pressurized gas through the nozzle using only the available enthalpy of the propellant without any combustion, heat addition, or other mechanisms to add energy [2].

There are three different cold gas propulsion system configurations according to their operating principle. These are pressurized gas systems, heated gas systems and liquified gas systems, and their general schematics are provided in Fig. 2. Pressurized gas systems are the simplest among the three considering the operating principle, and the propulsion system examined in this study is the first one of these three.

The operation principle of a cold gas propulsion system is reasonably straightforward. The main propellant tank is filled with a highly pressurized (~ 30 MPa) gas propellant. The pressurized propellant is kept in the tank with the help of a latch valve. After initiating the operation of the propulsion system, a pressure regulator is used to decrease the high pressure to the operational levels (~1 MPa). The gas flow is controlled by the solenoid valves before the thruster. Once the solenoid valves are activated, high pressurized propellant gas is expanded and accelerated through the nozzle, and the desired thrust is obtained.

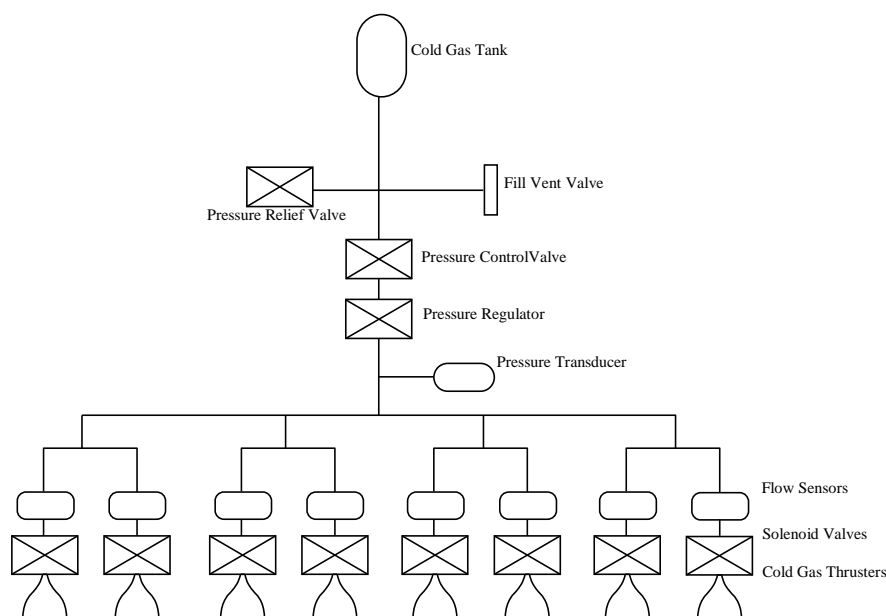


Figure 1. Schematic drawing of a cold gas propulsion system with main components. Recreated after Anis [Anis, 2012]

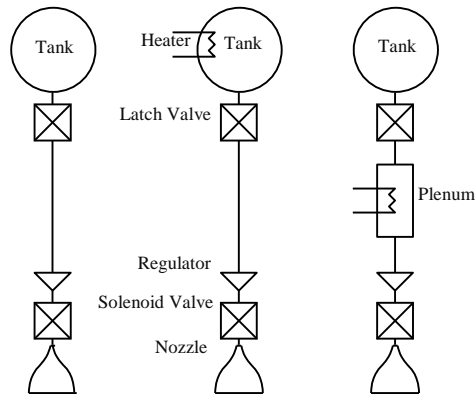


Figure 2. Cold gas propulsion systems from left to right; pressurized, heated and liquefied gas systems. Recreated after Lev. [Lev et al., 2014]

It is possible to find many successful cold gas propulsion systems in operation in the literature. Two Canadian-based cold gas propulsion system applications were studied and launched successfully in 2008 and 2014 in the nanoscale satellite experimental program CanX (Canadian Advanced Nanospace eXperiment). CanX-2 was using Nano Propulsion System (NANOPS) in April 2008 [Sarda et al., 2008] while CanX-5 was using the Canadian Nanosatellite Advanced Propulsion System (CNAPS) and sulfur hexafluoride had chosen as the propellant for both propulsion systems [Risi, 2014]. The propulsion system designed for Microelectromechanical System PICOSAT Inspector was using Xenon as the propellant [Hinkley, 2008]. Propulsion Operation Proof SATellite – High Performance 1 (POP AT-HIP1), which had Argon-based thrusters were fired successfully in 2014 [Manzoni et al., 2015].

Propellant selection is an essential step in the design of the propulsion system since it directly affects both the propellant tank and thruster design. Moreover, using a contamination-free propellant is crucial, considering that it may affect the sensing devices and mechanical actuators with their residues [Bzibziak, 2000]. Considering the propellant tank design parameters in terms of handling and storage, using a propellant, which has a moderately low boiling point, low melting temperature and mass-efficient, is generally preferred [Jerman et al., 2011]. There are many options for gaseous propellants, including hydrogen, helium, Nitrogen, Argon, Xenon. However, due to its storage density, performance, cost-effectiveness, and contamination-free nature, Nitrogen has been used in this study.

Thruster design is one of the most critical phases of the overall design process of the propulsion system since this component is responsible for delivering the desired performance. A thruster is typically the combination of the thrust chamber and the nozzle. Thrust chamber design is crucial since it determines the thrust delay following the actuation of the thruster valve. Nozzle design should also be performed carefully, since this is the part where the flow is accelerated and the desired thrust is obtained. Cold gas thrusters generally have converging or

converging-diverging (De Laval) nozzle configurations. The aim of obtaining higher performance led to the use of De Laval nozzles widely in thrusters. De Laval nozzle is designed such that flow through its throat reaches sonic velocity to maximize the allowable mass flow rate and hence to maximize the allowable thrust. There are two options for the divergent part of these nozzles, conical or bell-shaped. Since the physical dimensions of these thrusters are exceedingly small, conical nozzles are preferred for practical applications by taking into account the ease of manufacturing and design procedure. The nozzle used in the scope of this study is also designed to include a conical and divergent section. The main design parameter, half cone angle (α), has been chosen as 15° by comparing the performance of 8° , 15° , and 25° half cone angles.

CURRENT STUDIES IN THE LITERATURE

There are many studies in the literature to evaluate the performance of a cold gas thruster using both numerical and experimental approaches. Matticari et al. (2010) conducted experimental and numerical studies on a cold gas system in which Xenon was used as the propellant. CFD simulations were performed for the 2D axisymmetric flow domain with commercial software, including the viscous effects. Pressure and velocity contours are provided in their article.

Nozzle exit pressure and temperature are obtained as 21 Pa and 12.40 K [Matticari et al., 2010]. These cryogenic values give rise to a question of the possibility of phase change of the propellant at any location of the flow inside the nozzle. A related experimental study was performed in the vacuum chamber facility at the European Space Research and Technology Centre (ESTEC) Electronic Propulsion Laboratory. During the performance tests, mass flow rate, gas inlet temperature and pressure measurements were taken. In the case of a phase change, it was expected to observe a loss in thrust compared to the estimated value. However, experimental results did not show any reduction in nozzle performance. A similar result was obtained for a cold gas thruster, which uses compressed air as the propellant, by Ranjan et al. (2017). Numerical simulation showed that the nozzle exit temperature approximately 35 K for vacuum conditions. Corresponding experiments that were conducted in a vacuum chamber showed that the expected thrust and specific impulse values were reached.

Another important issue to be proved was the capability of SU2 to solve problems, including real gas models. A numerical comparison was performed to simulate the flow in a nozzle to show whether SU2 was capable of solving real gas equations for nozzle applications. Navier-Stokes equations were solved by using the second-order Roe scheme and implicit Euler algorithm based on CFL adaptation [Pini et al., 2017]. Comparison has been performed between the results of SU2 and ANSYS-CFX using the Span-Wagner equation of state. The authors provided both the Mach and pressure ratio contours. The results of both simulations were matching

reasonably well. These results show that SU2 is an appropriate solver for the cold gas thruster simulations.

Experimental test setups are also widely presented in the literature. One of the most related experimental procedures has been performed for the design and testing of Pakistan's first cold gas propulsion system (PRSS) prototype. The propellant of this system was chosen as Nitrogen, and it has eight 1 N thruster, which operates at a chamber pressure of 8 bar (0.8 MPa) [Anis, 2012]. Thrusters employed in this prototype were conical nozzles with a 16° half-angle and an area ratio of 50:1, and the nozzle efficiency was taken as 98% [Anis, 2008, 2012]. An experimental test campaign has been designed by using load cells for the force measurements. The specific impulse was measured as 73 s for continuous operation as a result of the tests, which was the expected value.

Another experimental study of a cold gas thruster was performed by Rickermers (2004). The vacuum chamber at the University of Bremen's Hochschule Hyperschall Kanal was used. The chamber has a volume of 1.5 m³, and the minimum achievable pressure level is 10 to 3 mbar (1000 to 300 Pa). Besides the Schlieren visualization technique, pressure and temperature sensors were used to track down the flow through the nozzle. The authors provided pressure and thrust test results.

Pressure readings show that the pressure inside the vacuum chamber increases following the thruster operation as expected. Another outcome is while the chamber pressure is constant, thrust decreases in continuous operation. It was concluded that the first reason might be maintaining larger ambient pressure at the nozzle exit than the theoretical calculations. Additionally, it was considered that the boundary layer at the throat might decrease the mass flow rate, which may result in having lower thrust values. Another reason behind this might be the decrease in specific impulse due to the decrease in the temperature following the continuous operation.

METHODOLOGY

Flow field simulations are performed by employing an open-source solver considering their flexibility compared to commercial software. The Middle East Technical University Mechanical Engineering CFD group has a strong background in SU2. Hence SU2 is chosen as the platform for the flow simulations. SU2 is capable of solving multi-physics Partial Differential Equation (PDE) problems and PDE constrained optimization problems on unstructured meshes. The mesh generation flow diagram is provided in Fig. 3. The mesh generation has been performed in Salome, yet since its output is not compatible with the SU2 native mesh format, Gmsh and enGrid open source software are used.

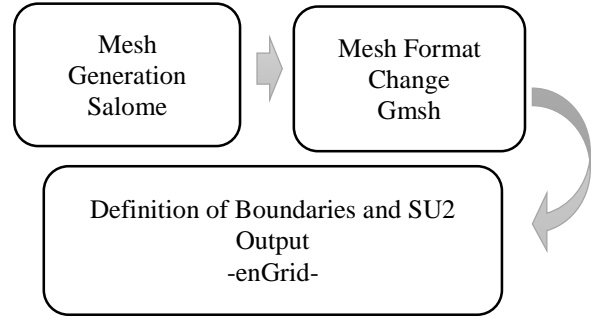


Figure 3. Tools used for SU² native mesh generation

Compressible Gas Models

Developers of SU2 coupled a built-in thermodynamic library with the main solver considering the non-ideal gas applications. Ideal gas, van der Waals and Peng-Robinson gas models are the available thermodynamic models embedded in the code. In this section, the capabilities of these models are investigated.

Ideal Gas Thermophysical Model: This model describes the volumetric and caloric behaviour of the polytropic ideal gas.

$$\begin{cases} p(T, v) = \frac{RT}{v} \\ e(T, v) = e(T) = e_{\text{ref}} + c_v(T - T_{\text{ref}}) \\ s(T, v) = s_{\text{ref}} + c_v \ln \frac{T}{T_{\text{ref}}} + R \ln \frac{v}{v_{\text{ref}}} \\ c_v = \frac{1}{\gamma - 1} R \end{cases} \quad (1)$$

where p is the pressure, T is the temperature, R is the gas constant, v is the specific volume, e is the total energy per unit mass, and s is the total entropy per unit mass. γ is the ratio of specific heats and can be expressed as $\gamma = c_p / c_v$ where c_p is the heat capacity at constant pressure and c_v is the heat capacity at constant volume. These sets of equations are calculated based on reference energy and entropy. Reference energy and entropy are defined as follows:

$$\begin{cases} e_{\text{ref}} = c_v T_{\text{ref}} \\ s_{\text{ref}} = -c_v \ln T_{\text{ref}} + R \ln v_{\text{ref}} \end{cases} \quad (2)$$

Reference temperature and specific volume are defined by the user according to the reference pressure. These values are used to non-dimensionalize the problem. The following form of the equations is obtained.

$$\begin{cases} e(T, v) = c_v T \\ s(T, v) = c_v \ln T + R \ln v \end{cases} \quad (3)$$

In order to be used in the numerical schemes, derivatives are given in Eqn. (4) to (7) should be calculated for the ideal gas thermodynamic equation of state.

$$\left(\frac{\partial p}{\partial e}\right)_\rho = (\gamma - 1)\rho \quad (4)$$

$$\left(\frac{\partial p}{\partial \rho}\right)_e = (\gamma - 1)e \quad (5)$$

$$\left(\frac{\partial T}{\partial e}\right)_\rho = \frac{(\gamma - 1)}{R} \quad (6)$$

$$\left(\frac{\partial T}{\partial \rho}\right)_e = 0 \quad (7)$$

where ρ is the density. The final step is the calculation of the speed of sound, c as

$$c^2 = \left(\frac{\partial p}{\partial \rho}\right)_e + \frac{p}{\rho^2} \left(\frac{\partial p}{\partial e}\right)_\rho \quad (8)$$

van-der Waals Gas Thermophysical Model: The set of equations for this thermophysical model is provided in Eq. (9).

$$\begin{cases} p(T, v) = \frac{RT}{v - b} - \frac{a}{v^2} \\ e(T, v) = c_v T - \frac{a}{v} \\ s(T, v) = c_v \ln T + R \ln(v - b) \end{cases} \quad (9)$$

Two new coefficients are introduced in this model. These coefficients are dependent on the chemical composition and gas properties. The coefficient a is the measure of the intensity of the intermolecular attraction force. The coefficient b is the co-volume, which represents the volume of the atoms or molecules in one mole of the gas. These coefficient are given as

$$\begin{cases} a = \frac{27 R^2 T_{cr}^2}{64 p_{cr}} \\ b = \frac{1 R T_{cr}}{8 p_{cr}} \end{cases} \quad (10)$$

Constants a and b are dependent on critical temperature and the pressure of the propellant. For the sake of consistency, energy and entropy equations are defined as in the ideal gas model. Here T_{cr} and p_{cr} are the critical pressure and temperature. The critical point is unique in the $(p - T - v)$ phase diagram, where both $(dp/dv)_T$ and $(d^2p/dv^2)_T$ are zero. The critical point is related to the size of the atom. Around the critical point, the distance between gas atoms becomes small as the molecules almost touch each other. Then a strong short-range repulsive force between gas atoms becomes significant. This force is correlated to b , which is roughly equal to the volume of a gas molecule.

Thermodynamic derivatives are also calculated in terms of coefficients a and b , as shown in equations (11) to (14).

$$\left(\frac{\partial p}{\partial e}\right)_\rho = \frac{(\gamma - 1)\rho}{1 - \rho b} \quad (11)$$

$$\left(\frac{\partial p}{\partial \rho}\right)_e = \frac{(e + 2\rho a - \rho^2 ab)}{\rho(1 - \rho b)} \left(\frac{\partial p}{\partial e}\right)_\rho - 2\rho a \quad (12)$$

$$\left(\frac{\partial T}{\partial e}\right)_\rho = \frac{(\gamma - 1)}{R} \quad (13)$$

$$\left(\frac{\partial T}{\partial \rho}\right)_e = \frac{1}{a} \left(\frac{\partial T}{\partial e}\right)_\rho \quad (14)$$

In order to calculate the speed of sound, Eq.(8) is utilized.

Peng-Robinson Gas Thermophysical Model: The model modifies the Soave-Redlich-Kwong(SRK) equation of state. The model is developed to improve the predictions for liquid density, vapor pressure and equilibrium ratio. The set of equations is to be solved in this model is provided in Eqn. (15).

$$\begin{cases} p(T, v) = \frac{RT}{v - b} - \frac{a\alpha^2(T)}{v^2 + 2bv - b^2} \\ e(T, v) = c_v T - \frac{a\alpha(T)(k + 1)}{b\sqrt{2}} \tanh^{-1} \frac{b\sqrt{2}}{v + b} \\ s(T, v) = c_v \ln T + R \ln(v - b) - \frac{a\alpha(T)k}{b\sqrt{2}T T_{cr}} \tanh^{-1} \frac{b\sqrt{2}}{v + b} \end{cases} \quad (15)$$

For this model, parameters of $\alpha(T)$, a and b have to be defined. $\alpha(T)$ is the measure of the intermolecular attraction force, and it is temperature-dependent. As mentioned in the van-der Waals gas model, coefficients a and b depend on both the critical temperature and pressure.

$$\begin{cases} a = 0.45724 \frac{(RT_{cr})^2}{p_{cr}} \\ b = 0.0778 \frac{RT_{cr}}{p} \\ \alpha(T, \omega) = \left[1 + k \left(1 - \sqrt{\frac{T}{T_{cr}}} \right) \right] \\ k = \begin{cases} 0.37464 + 1.54226\omega - 0.26992\omega^2 & \omega \leq 0.49 \\ 0.379642 + 0.48503\omega - 0.164423\omega^2 + 0.016666\omega^3 & \omega > 0.49 \end{cases} \end{cases} \quad (16)$$

As can be seen from the above equations, $\alpha(T)$ depends both on temperature and the acentric factor, which is a function of the saturated vapor pressure and the critical pressure. This parameter also varies with the chemical composition of the gas. Entropy and energy equations are defined as the same as the ideal gas model to satisfy consistency.

The solution of thermodynamic derivatives is more challenging compared to the other gas models. First, the second derivatives are provided in Eqn. (17) to (20):

$$\left(\frac{\partial p}{\partial e}\right)_\rho = \frac{\left(\frac{\partial p}{\partial T}\right)_\rho}{\left(\frac{\partial e}{\partial T}\right)_\rho} \quad (17)$$

$$\left(\frac{\partial p}{\partial \rho}\right)_e = \left(\frac{\partial p}{\partial \rho}\right)_T - \left(\frac{\partial p}{\partial e}\right)_\rho \left(\frac{\partial e}{\partial \rho}\right)_T \quad (18)$$

$$\left(\frac{\partial T}{\partial e}\right)_\rho = \frac{1}{\left(\frac{\partial e}{\partial T}\right)_\rho} \quad (19)$$

$$\left(\frac{\partial T}{\partial \rho}\right)_e = \left(\frac{\partial T}{\partial \rho}\right)_p - \left(\frac{\partial T}{\partial p}\right)_\rho \left(\frac{\partial e}{\partial T}\right)_p \quad (20)$$

The complexity of the second derivatives is due to the fact that the coefficient α depends both on the temperature and the acentric factor. Hence, partial derivatives are implemented as in Eqn. (21) and (22):

$$\left(\frac{\partial p}{\partial T}\right)_\rho = \frac{R}{(v-b)} - \frac{2a\alpha'}{[v(v+b) + b(v-b)]} \quad (21)$$

where

$$\alpha' = \frac{d\alpha}{dT} \quad (22)$$

According to the information provided above, partial derivatives are calculated as in Eqn. (23) to (30).

$$\left(\frac{\partial e}{\partial T}\right)_\rho = \frac{R}{(\gamma-1)} - \frac{a}{b\sqrt{2}} \left[2\alpha\alpha' + k\alpha' \sqrt{\frac{T}{T_{cr}}} + \frac{1}{2}k\alpha(TT_{cr})^{-0.5} \right] f(v) \quad (23)$$

$$\begin{aligned} \left(\frac{\partial p}{\partial \rho}\right)_T &= -\frac{1}{\rho^2} \left(\frac{\partial p}{\partial v}\right)_T \\ &= -\left(-\frac{RT}{(v-b)^2} + \frac{2a\alpha'(v+b)}{[v(v+b) + b(v-b)^2]} \right) v^2 \end{aligned} \quad (24)$$

$$\begin{aligned} \left(\frac{\partial e}{\partial \rho}\right)_T &= -\frac{a\alpha(T)}{b\sqrt{2}} \left[\alpha(T) + k \sqrt{\frac{T}{T_{cr}}} \frac{b\sqrt{2}}{a + 2\rho b - \rho^2 b^2} \right] \end{aligned} \quad (25)$$

$$\left(\frac{\partial \rho}{\partial T}\right)_p = -\rho^2 \left(\frac{\partial v}{\partial T}\right)_p \quad (26)$$

$$\left(\frac{\partial T}{\partial \rho}\right)_p = \frac{1}{\left(\frac{\partial \rho}{\partial T}\right)_p} \quad (27)$$

$$\left(\frac{\partial v}{\partial T}\right)_p = -\left(\frac{\partial p}{\partial v}\right)_T^{-1} \left(\frac{\partial p}{\partial T}\right)_v \quad (28)$$

$$\left(\frac{\partial e}{\partial T}\right)_p = \left(\frac{\partial h}{\partial T}\right)_p - p \left(\frac{\partial v}{\partial T}\right)_p \quad (29)$$

$$\left(\frac{\partial h}{\partial T}\right)_p = \left(\frac{\partial e}{\partial T}\right)_v + T \left(\frac{\partial p}{\partial T}\right)_v \left(\frac{\partial v}{\partial T}\right)_p \quad (30)$$

Finally, the speed of sound is calculated again, according to Eq.(8).

Experimental Test Setup

A series of performance tests for the cold gas propulsion system have been performed to observe the characteristics of the system. The challenging part of these experiments is the simulation of very low pressure to simulate space conditions. In order to satisfy operation conditions, a vacuum chamber test campaign is used. This facility is designed and manufactured by national resources and by Turkish sub-contractors. The test facility, which is shown in Fig. 4, has a vacuum chamber of 3.1 m³, and the desired low-pressure environment is maintained by using vacuum pumps. The vacuum chamber has the ability to depressurize down to 5 Pa. Real-time pressure and temperature sensors are located inside the chamber to observe the chamber conditions.



Figure 4. Thrust chamber test setup

The test setup contains a propellant tank, a commercial regulator, a fill-drain system, a manifold, a thruster valve and the thruster itself, which is fitted by the required pressure and temperature sensors. Schematic drawing, which can be seen in Fig. 5, shows the test setup clearly. Pressure measurements are taken from the propellant tank exit, regulator and manifold downstream, thruster

valve upstream and thrust chamber. The temperature readings are taken from both the tank exit and the thrust chamber. The propellant tank, which is made from 4130 steel and painted to prevent corrosion, is pressurized by using a compressor booster. A 44-1362 series TESCOM regulator is used to lower the propellant pressure to the operating level. A thruster valve is basically a solenoid valve that operates at 28 V DC and 1 A. Pressure measurements from the thrust chamber have been taken by using a Kulite HKM-375 series pressure sensor. TRAFIQ EPI400.0A 8287 pressure transmitters are used for the rest of the pressure sensors. The precision load cell of Burster 9431 series is used. The load cell has the capability to measure forces up to 500 N. Experimental test setup inside the vacuum chamber is given in Fig. 6.

A thrust frame is designed to transfer the produced thrust to the load cell. Alignment of the thrust vector and the load cell is taken into account during the design process in order to prevent the measurement of the side loads. Connection through the vacuum chamber is accomplished by using a flexible hose in order not to affect the thrust measurements.

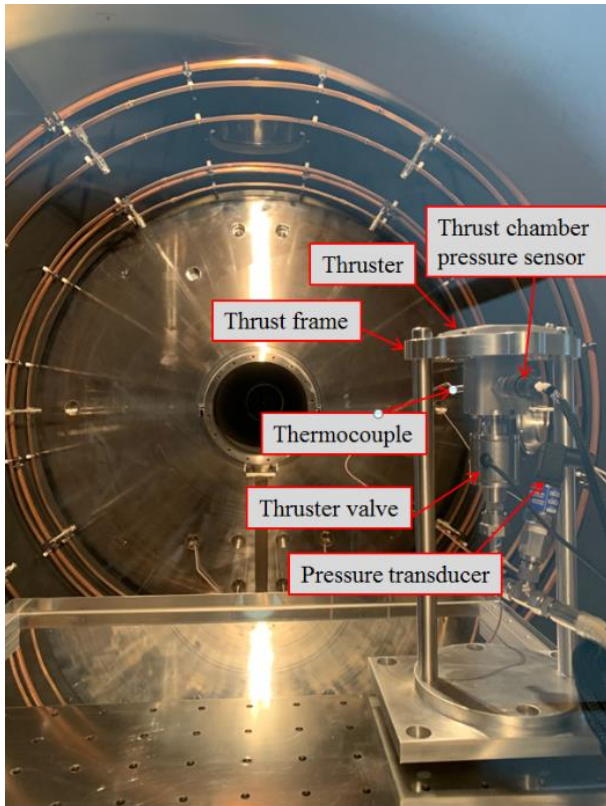


Figure 5. Thruster and thrust frame inside the vacuum chamber

THRUSTER DESIGN

The thruster is the main component responsible for satisfying the performance requirements of the propulsion system. Thrusters that operate in space are designed to provide optimum expansion performance in vacuum conditions, which means infinite expansion. A realistic design procedure includes the decision of the

outlet pressure, which determines the produced thrust. Thrust chamber pressure is another critical parameter since it affects the propellant tank weight and also the pipeline weight. Since it is desired for systems to be as light and compact as possible, thruster design becomes more crucial. Thrust for an ideal gas and expansion to an ambient pressure p_a is calculated as follows [Dorado Et. Al. 2013]:

$$F = A_t p_c \gamma \left[\left(\frac{2}{\gamma - 1} \right) \left(\frac{2}{\gamma + 1} \right)^{\frac{\gamma - 1}{\gamma + 1}} \left\{ 1 - \left(\frac{p_e}{p_c} \right)^{\frac{\gamma - 1}{\gamma}} \right\}^{\frac{1}{2}} + (p_e - p_a) A_e \right] \quad (31)$$

In this equation, F is the thrust, A_t is the throat area, p_c is the chamber pressure, A_e is the nozzle exit area, p_e is the nozzle exit pressure, p_a is the ambient pressure, and γ is the ratio of specific heats. Exit pressure for the nozzle might be chosen by considering the lowest altitude at which the thruster starts its operation. This is because lowering the exit pressure results in longer and heavier nozzles, which is not desired for the overall propulsion system. Determination of the chamber pressure is also important. It is clear that higher chamber pressure will result in higher performance, yet it requires a heavier thruster. Considering the weight and performance optimization of the nozzle, we have chosen 1.0 MPa (10 bar) and 300 Pa as the chamber pressure and nozzle exit pressure, respectively.

The pressure difference between nozzle exit and ambient pressure is small, as well as the nozzle exit area, the contribution of pressure to the thrust is negligible compared to momentum thrust. The thrust equation can be expressed in Eqn. (32) which shows the relation of mass flow rate, exit velocity, and specific impulse. Determining the mass flow rate will lead to geometrical parameters of the thruster.

$$F = \dot{m} V_e \quad (32)$$

\dot{m} is the mass flow rate which is maximized when the Mach number at the throat reaches unity, and V_e is the nozzle exit velocity. The next step is the calculation of nozzle exit velocity to determine the mass flux rate since the desired thrust is already known as 10 N. Nozzle exit velocity can be found through the following relation.

$$V_e = \lambda_n \sqrt{\left(\frac{2\gamma}{\gamma - 1} \right) R T_c \left[1 - \left(\frac{p_e}{p_c} \right)^{\frac{\gamma - 1}{\gamma}} \right]} \quad (33)$$

For the current thruster design, chamber pressure and temperature are taken as 1 MPa and 293 K, respectively. The gas constant for the propellant, Nitrogen, is taken as 296.8 J/kg K, and the specific heat ratio is taken as 1.4. The nozzle efficiency, λ_n , includes losses in the nozzle and taken as 95%. At the end of the nozzle, the exit

velocity is calculated as 704 m/s. The mass flow rate is calculated as 14.2 g/s to satisfy the desired thrust level. The nozzle exit area can be obtained by using the design values through Eqn. (34).

$$\frac{\dot{m}}{A_e} = \sqrt{\frac{\gamma}{RT_c}} p_c \sqrt{\left(\frac{2\gamma}{\gamma-1}\right) \left[\left(\frac{p_e}{p_c}\right)^{\frac{2}{\gamma}} - \left(\frac{p_e}{p_c}\right)^{\frac{\gamma+1}{\gamma}} \right]} \quad (34)$$

Nozzle exit diameter is obtained as 520 mm² and the corresponding nozzle exit diameter is found as 25.7 mm. To obtain the throat area, first, the nozzle exit Mach number has to be obtained. The exit Mach number is calculated as 6.76 using the chamber pressure and nozzle exit pressure. Finally, the expansion ratio is obtained as 84, which corresponds to the nozzle throat diameter of 2.8 mm from the following relation.

$$\frac{A_e}{A_t} = \frac{1}{M_e} \left\{ \left(\frac{2}{\gamma+1} \right) \left(1 + \frac{\gamma-1}{2} M_e^2 \right) \right\}^{\frac{\gamma+1}{2(\gamma-1)}} \quad (35)$$

The thrust chamber diameter is determined considering the thruster valve exit cross-section in order not to suffer from pressure loss. The length of the thruster is decided to fit the overall propulsion system. Fig. 7 shows the final thruster geometry.

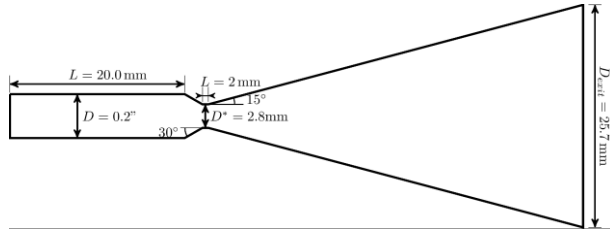


Figure 6. Thruster dimensions

RESULTS

The operational environment of the cold gas thrusters is space that has extremely low pressure. In addition, the nature of the propulsion system results in having cryogenic temperature and pressure values, which give rise to the question of whether the continuum postulate is still valid or not. This is also necessary for the sake of the numerical simulations to check the validity of the applicability of Navier-Stokes equations.

Continuum Postulate Validation

The non-dimensional Knudsen number, Kn, is used to decide whether the continuum postulate is valid or not. Knudsen Number is defined as the ratio of the molecular mean free path of fluid to the characteristic length of the flow field [Greer et al., 1967].

$$Kn = \frac{\text{Molecular mean free path}}{\text{Characteristic linear dimension of the flow field}} \quad (36)$$

Even though the Knudsen number is desired to be as close to zero as possible, in order for the continuum postulate to be valid, it should be less than approximately 0.01 [Aksel, 2011].

In order to calculate the Knudsen number, first, the molecular mean free path (MFP) of the fluid should be calculated. MFP, λ , is the distance traveled by a molecule between two consecutive collisions and can be calculated as follows:

$$\lambda = \frac{k_B T}{\sqrt{2} \pi p d_m^2} \quad (37)$$

In the above equation, k_B is the Boltzmann constant (1.38064910-23 J/K) and d_m is the molecular diameter of the gas. The outlet of the thruster is the section in which the lowest temperature and pressure values are expected. As a result, to calculate the MFP, the outlet pressure of 300 Pa and corresponding outlet temperature of 28.9 K are used. The molecular diameter of the Nitrogen is taken as 3.64 Å [Kentish et al., 2008]. Corresponding MFP is obtained as 2.2594x10⁻⁶ m. Since the nozzle outlet is decided as the critical section, the nozzle diameter is taken as the characteristic length. Design procedure gives the nozzle outlet diameter as 25.7x10⁻³m and the corresponding Kn is calculated as 8.79x10⁻⁵. Since it is lower than the critical value of 0.01, it is clear that the continuum postulate is applicable to this problem.

Thruster Nozzle Verification

The first step is the generation of the computational grid in order to capture the physics of the problem correctly. Grid sizing and distribution is important for the accuracy and stability of the solution. For the mesh generation, the unstructured NETGEN 1D-2D-3D grid generator in Salome is used. Mesh independency analysis has been conducted by applying the nominal operation conditions and solving Euler equations to the grid sizes of 13732, 49468, 114399, 506172, 1240249, and 5356379.

Table 1. Mesh verification study results

Mesh size	\dot{m} per area [kg/m ² s]	% Error in \dot{m} per area
13732	2321.4	1.84
49468	2248.3	4.93
114399	2392.3	1.16
506172	2324.9	1.69
1240249	2319.9	1.90
5356379	2313.6	2.29

Table 1 compares the mass flow rate through the nozzle for different mesh densities. As a result of this comparison, the grid having 114,399 cells is decided to be used for the rest of the simulations.

Nominal Operational Conditions: The first set of comparisons has been performed for the nominal

operating condition of the thruster, which is 1MPa of chamber pressure and 293 K of the propellant temperature.

Vacuum chamber performance test results for thrust chamber pressure and the thrust are provided in Fig. 8. Following the thruster valve actuation, both the pressure inside the chamber and the thrust value increase. It is seen that the pressure inside the chamber reaches the steady-state value of 1.05 MPa in 3 ms. The difference of 50 kPa between the expected and experimental value is due to the imprecise adjustment of the mechanical pressure regulator. In idle condition, 35 N of thrust reading is observed. This non-zero force reading is due to the overall weight of the thruster, sensors and thrust frame. After the actuation of the thruster valve, a steady-state thrust value of 45 N is obtained. The difference between the idle and when the thruster on conditions reads 10 N, which is the expected value.

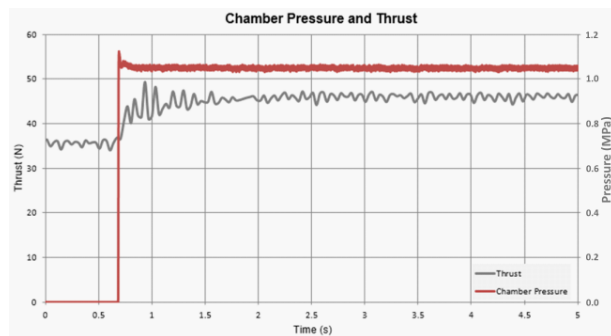


Figure 7. Nominal operating conditions vacuum chamber test results for chamber pressure (red line) and thrust (gray line)

Experimental measurements are applied as the initial and boundary conditions for the numerical simulations. Chamber pressure and gas temperature values of 1 MPa and 293 K are defined as the initial conditions at the inlet. The environmental pressure and temperature values of 200 Pa and 293 K, respectively, similar to the pressure-outlet boundary conditions, are defined as the initial conditions.

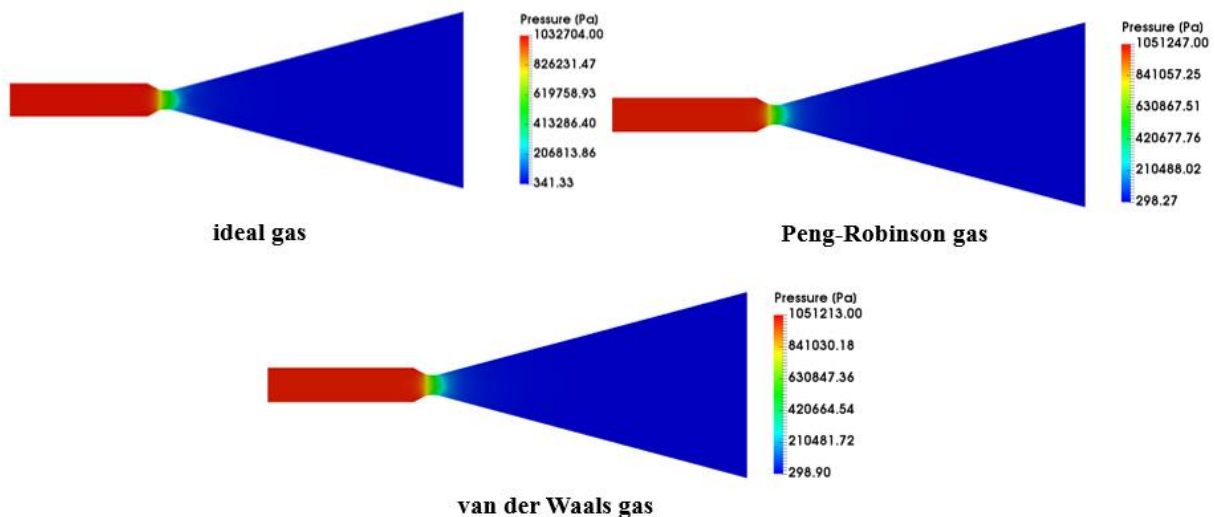


Figure 8. Nominal temperature operation condition results for different gas models

Euler equations are solved with the Roe flux splitting scheme. For real gas models, additional Riemann boundary conditions are defined in the SU2 configuration file. A CFL adaptation between 0.4 and 5 is used to obtain faster convergence.

Numerical simulation results are provided in Fig. 9 for the three gas models. In general, real gas models predicted higher chamber pressures compared to the ideal gas model. Again, the pressure at the outlet section obtained from real gas models is closer to the design value compared to the ideal gas result.

Another comparison is performed in terms of thrust. Thrust is calculated by the area integration at the nozzle outlet section by using the open-source visualization tool, ParaView. As shown in Table 2, the real gas models predicted closer thrust values compared to the design values.

Table 2. Thrust comparison between gas models

Gas Model	Thrust [N]	% Error in Thrust	Solution Time [min]
Ideal Gas	10.86	+8.6	600
van-der Waals	9.31	-6.9	170
Peng-Robinson	9.31	-6.9	159

In the preliminary design phase, it is crucial to obtain the fastest solution as well as the most accurate one. Therefore, the final comparison of the model performance has been carried out for the computational time. The ideal gas simulation takes approximately 600 minutes to converge, while Peng-Robinson takes approximately 170 minutes. The fastest convergence is obtained with the van-der Waals gas model within 159 minutes. It should be noted that the ideal gas model overpredicts the thrust, while real gas models underpredict it.

Low-Temperature Operational Conditions: Low-temperature operation conditions are for a chamber pressure of 1 MPa and a propellant temperature of 243 K. For low-temperature conditions, initially, the propellant inside the tank is thermally conditioned to 262 K by using a thermal chamber in. Then, to obtain 243 K in the chamber, additional depressurization is performed by discharging the propellant through extra flexible hoses attached to the manifold.

First, the results obtained from the performance test is provided in Fig. 10. Steady-state chamber pressure of 1 MPa is achieved at the beginning of the continuous operation. However, due to the sensitivity of the pressure regulator to low temperatures, the pressure inside the chamber is decreased during the operation. Prior to the thruster valve actuation, it can be seen that the load cell measures 34 N corresponding to the dead weight, as explained before. Steady-state measurement of the load cell reports 10 N of thrust for the low-temperature case.

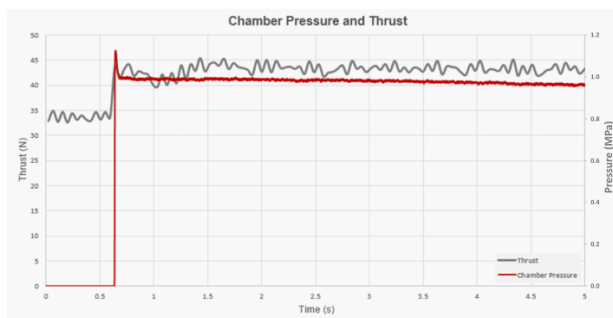


Figure 9. Low temperature operating conditions vacuum chamber test results for chamber pressure (red line) and thrust (gray line)

The same logic applies to the low-temperature numerical simulations as in nominal operating conditions. Chamber conditions of 1 MPa and 243 K are defined as the initial condition at the inlet, while vacuum chamber conditions of 200 Pa and 293 K are defined as for the nominal operating temperature case as the initial condition at the outlet section, respectively.

Simulations have been performed by using the same conditions as the nominal conditions. Euler equations with the Roe flux splitting scheme are used while additional Riemann boundary conditions are applied for the real gas models. CFL adaptation is also used in order to increase the convergence rate.

As seen from the results provided in Fig. 11, the real gas models predict closer values to the experiments when compared to the ideal gas model. When the temperature values are compared, it can be seen that the outlet temperatures obtained in this set of simulations are lower than the nominal temperatures. This is expected due to the lower temperature initialization at the inlet of the nozzle.

Thrust calculation is followed by temperature and pressure comparison. Results provided in Table 3 show that the ideal gas model predicts closer results to the experimental thrust value. However, considering that these simulations will be used in the preliminary design phase, prediction with an error of approximately 10% error can be considered as acceptable. Once again, the ideal gas model overpredicts the thrust, while real gas models underpredict it.

The reason for the thrust loss stems from the momentum thrust. Fig. 12 shows that the pressure change is not significant between the ideal gas and real gas models. Fig 13 shows the velocity variation through the nozzle. The momentum thrust reduces with the reduced exit velocity with real-gas models for the given inlet stagnation conditions and mass flow rate.

Table 3. Thrust comparison between gas models

Gas Model	Thrust [N]	% Error in Thrust	Solution Time [min]
Ideal Gas	10.44	+4.6	400
van-der Waals	9.01	-9.9	152
Peng-Robinson	9.01	-9.9	162

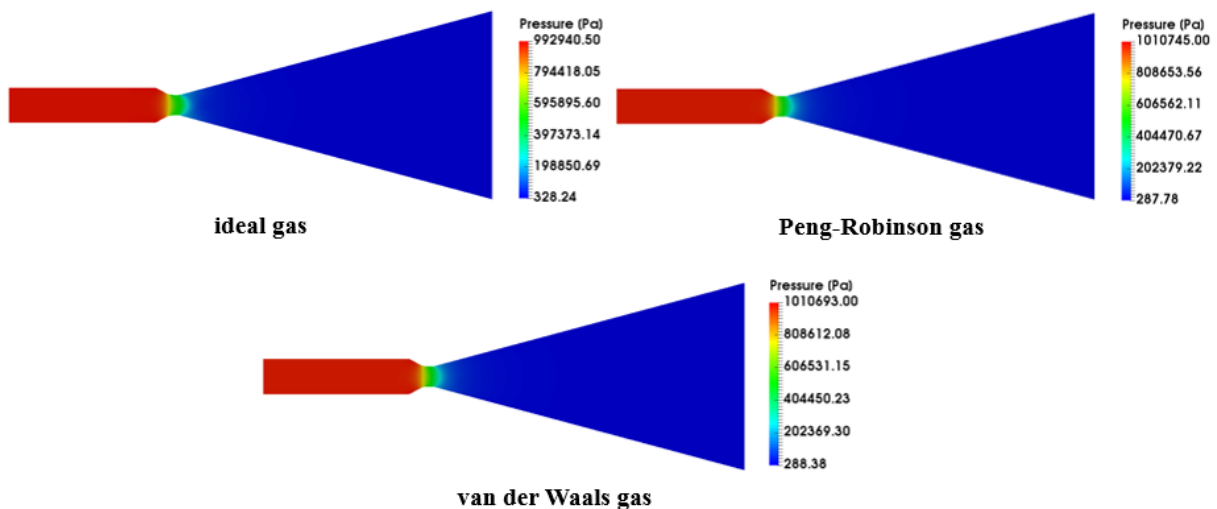


Figure 10. Low-temperature operation condition results for different gas models

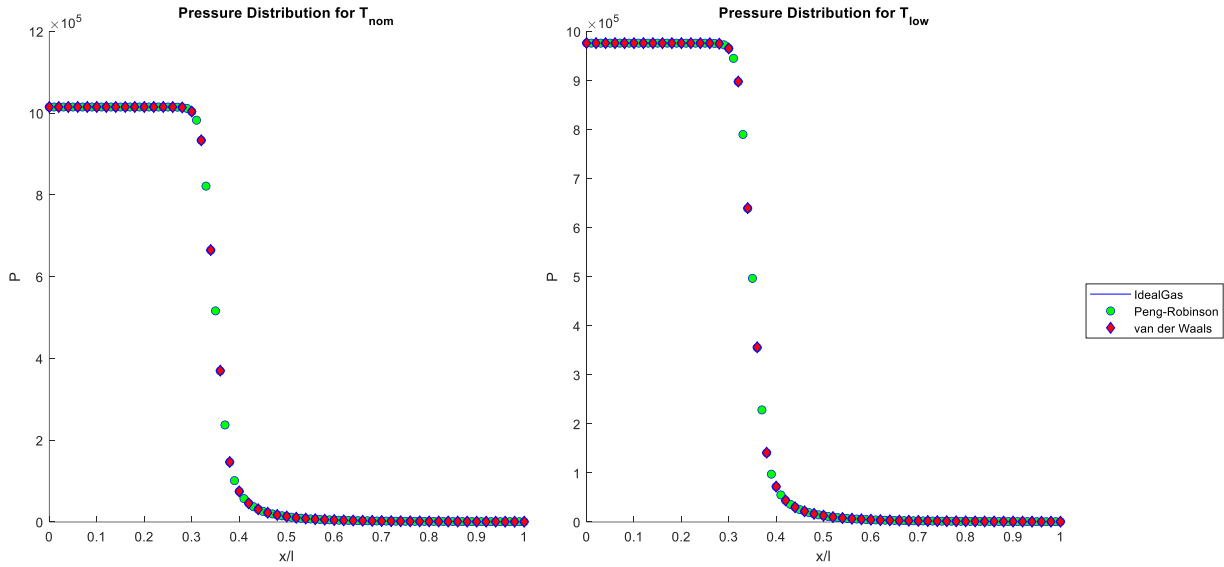


Figure 11. Center pressure solutions by different gas models

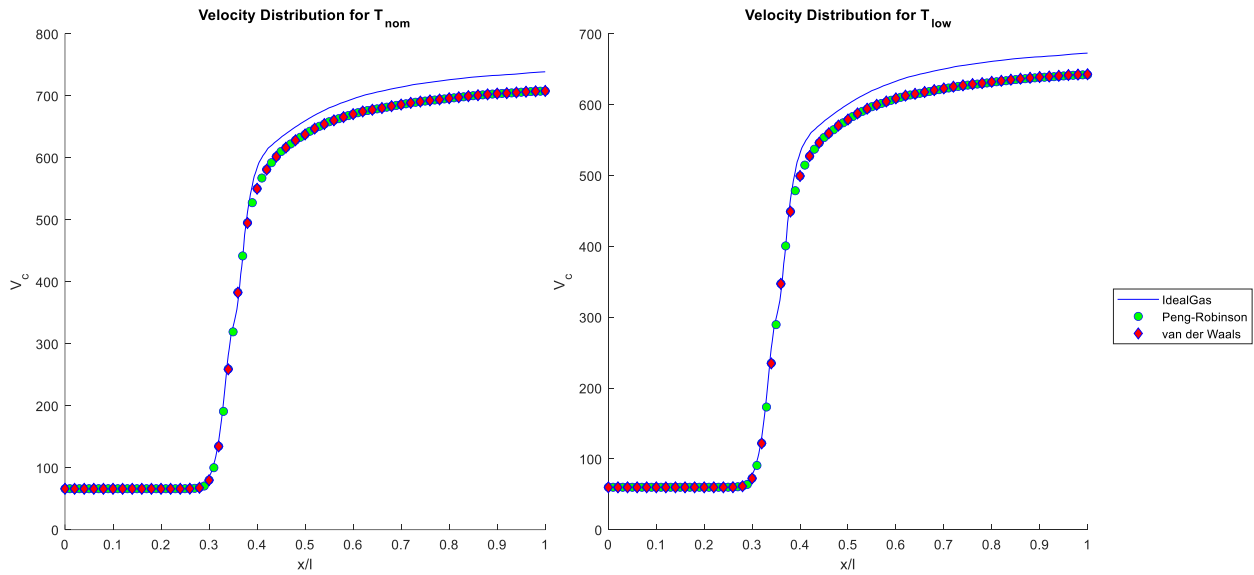


Figure 12. Center velocity solutions by different gas models

Last but not least, the computational time for each simulation is compared. Calculations are performed on a single core. The ideal gas simulation takes 400 minutes, while the Peng-Robinson gas model takes 162 minutes for convergence. For the van der Waals gas model, simulation time takes 152 minutes. It is seen that, for the van der Waals gas model, the percentage error observed in predicting the thrust is higher than the ideal gas model, yet the simulation time is much shorter. The main aim of the preliminary design phase is to obtain realistic performance predictions as fast as possible. Hence, the van der Waals gas model is preferred since it gives the performance predictions of the nozzle with an acceptable deficiency in the shortest time.

It is interesting to observe shorter solution times with real-gas models. The lower compressibility factor at lower temperatures makes the solution matrix less stiff. That allows larger pseudo-time steps and shorter convergence time. Also, during the expansion, the pressure and the

temperature drops, which results in less compressibility. This shows less expansion than a real gas. Less expansion simply results in less exit velocity, less exit pressure, and hence less thrust. Less expansion also means smaller flow gradients, hence improves the solution time.

CONCLUDING REMARKS

Experimental and numerical performance predictions of a cold gas thruster have been performed. The vacuum chamber facility utilized in this study has been employed for the experiments, while the open-source platform SU2 has been used for the numerical simulations. The effects of the utilization of different gas models already available in SU2 are investigated, and its impact is evaluated considering the requirements for the preliminary design phase.

The comparison of experimental and numerical simulations shows that the van der Waals gas model is

accurate enough to predict the performance of a cold gas thruster for both nominal and low-temperature operational conditions. Even though the thrust calculated for low-temperature simulations is lower than the experimental values, it is concluded that the performance predictions of this model satisfy the requirements for the preliminary design phase. Moreover, it is crucial to calculate the results quickly in addition to have accurate predictions. The van der Waals gas model provides the solution 2.5-4 times faster compared to the ideal gas model depending on the initial temperature condition. Even though the simulation duration is almost the same for the Peng-Robinson and the van der Waals gas models, still the van der Waals model is faster. Hence, since it allows us to compare many design alternatives in a very short period of time, the van der Waals gas model is favorable for companies. Another point that should be considered while assessing the simulation results at the preliminary design phase is that the ideal gas model tends to overpredict the net thrust, while real gas models tend to underpredict.

As mentioned before, Euler equations are solved in the scope of this study. Therefore, the effect of viscosity is neglected. Furthermore, turbulence is not included in the simulations. This becomes apparent in the low thrust predictions with real-gas models. With the current implementation of SU^2 we are not able to conduct unsteady, viscous real-gas simulations. For further studies, the effect of viscosity and turbulence can be investigated. Also, the real gas model implementations in SU^2 can be modified to improve the thrust predictions.

ACKNOWLEDGEMENTS

The experimental research in this project has been performed by the test facilities offered by ROKETSAN A.Ş. Authors like to show gratitude for the support.

REFERENCES

- Aksel, M. H., 2011, Fluid Mechanics. Middle East Technical University.
- Anis, A., 2012, Cold Gas Propulsion System - An Ideal Choice for Remote Sensing Small Satellites. *Remote Sensing - Advanced Techniques and Platforms, IntechOpen*.
- Anis, A., 2008, Design & Development of Cold Gas Propulsion System for Pakistan Remote Sensing Satellite (PRSS). *2nd International Conference on Advances in Space Technologies*, pp. 49–53, IEEE.
- Bzibziak, R., 2000, Update of Cold Gas Propulsion at MOOG. *36th AIAA/ASME/SAE/ASEE Joint Propulsion Conference and Exhibit*.
- Dorado, V., Grunder, Z., Schaefer, B., Sung, M., & Pedersen, K., 2013, NASA Marshall Space Flight Center Tri-gas Thruster Performance Characterization. *AIAA/ASME/SAE/ASEE Joint Propulsion Conference*
- Greer, H., & Griep, D.J., 1967, Dynamic Performance of Low-Thrust, Cold-Gas Reaction Jets in a Vacuum. *Journal of Spacecraft and Rockets*, vol. 4, no. 8, pp. 983–990.
- Hinkley, D., 2008, A Novel Cold Gas Propulsion System for Nanosatellites and Picosatellites. *22nd AIAA/USU Conference on Small Satellites*, Logan, UT.
- Jerman, T., & Langus, J., 2011, Calculating Cold Gas Microthruster Velocity Flow Using Finite Volume Analysis. University of Ljubljana, Ljubljana.
- Kentish, S.E., Scholes, C.A., & Stevens, G.W., 2008, Carbon Dioxide Separation Through Polymeric Membrane Systems for Flue Gas Applications. *Recent Patents on Chemical Engineering*, vol. 1, no. 1, pp. 52–66.
- Lemmer, K., 2017, Propulsion for Cubesats. *Acta Astronautica*, vol. 134, pp. 231–245.
- Manzoni, G., & Brama, Y. L., 2015, Cubesat Micropropulsion Characterization in Low Earth Orbit. *29th Annual AIAA/USU Conference on Small Satellites*.
- Matticari, G., Noci, G., Siciliano, P., Miccolis, M. & Strada, S., 2010, Cold Gas Thruster Assembly for SGEO Platform: Review of Development Activities by Thales Alenia Space Italia. *Space Propulsion Conference*, San Sebastian, Spain.
- Lev, R., Herscovitz, J., & Zuckerman, Z., 2014, Cold Gas Propulsion System Conceptual Design for the SAMSON Nano-satellite. *50th AIAA/ASME/SAE/ASEE Joint Propulsion Conference*, p. 3759.
- Pini, M., Vitale, S., Colonna, P., Gori, G., Guardone, A., Economon, T., Alonso, J., & Palacios, F., 2017, SU^2 : The Open-Source Software for Non-Ideal Compressible Flows. *Journal of Physics: Conference Series*, vol. 821, p. 012013, IOP Publishing.
- Ranjan, R., Chou, S., Riaz, F., & Karthikeyan, K., 2017, Cold Gas Micro Propulsion Development for Satellite Application. *Energy Procedia*, vol. 143, pp. 754–761.
- Rickmers, P., 2004, Performance Enhancement Through Flow Control in Cold Gas Thruster Nozzles. *55th International Astronautical Congress*.
- Risi, B. W., 2014, Propulsion System Development for the CanX-4 and CanX-5 Dual Nanosatellite Formation Flying Mission. University of Toronto.
- Sarda, K., Grant, C., Eagleson, S. Kekez, D., & Zee, R., 2008, Canadian Advanced Nanospace Experiment 2: n-orbit Experiences with a Three-kilogram Satellite. *22nd AIAA/USU Conference on Small Satellite*, Logan, UT.